

Pseudochemotactic drifts of artificial microswimmersPulak K. Ghosh,¹ Yunyun Li,^{2,*} Fabio Marchesoni,^{2,3} and Franco Nori^{4,5}¹*Department of Chemistry, Presidency University, Kolkata 700073, India*²*Center for Phononics and Thermal Energy Science, School of Physics Science and Engineering, Tongji University, Shanghai 200092, People's Republic of China*³*Dipartimento di Fisica, Università di Camerino, I-62032 Camerino, Italy*⁴*CEMS, RIKEN, Saitama, 351-0198, Japan*⁵*Physics Department, University of Michigan, Ann Arbor, Michigan 48109, USA*

(Received 22 April 2015; published 9 July 2015)

We numerically investigate the motion of active artificial microswimmers diffusing in a fuel concentration gradient. We observe that, in the steady state, their probability density accumulates in the low-concentration regions, whereas a tagged swimmer drifts with velocity depending in modulus and orientation on how the concentration gradient affects the self-propulsion mechanism. Under most experimentally accessible conditions, the particle drifts toward the high-concentration regions (pseudochemotactic drift). A correct interpretation of experimental data must account for such an “anti-Fickian” behavior.

DOI: [10.1103/PhysRevE.92.012114](https://doi.org/10.1103/PhysRevE.92.012114)

PACS number(s): 05.40.Jc, 82.70.Dd, 47.63.Gd, 87.17.Jj

I. INTRODUCTION

Chemotaxis, defined as the movement of motile cells or organisms in response to a chemical gradient, is a well-studied phenomenon [1]. Bacteria and other single- or multicellular organisms propel themselves up or down the concentration gradient of a particular substance in their search for nutrients or to avoid antagonists. Inspired by chemotaxis in biology, researchers synthesized artificial microswimmers [2,3] that can move in response to a chemical stimulus [4,5]. They showed that Janus particles (JP), in the form of two-faced Au-Pt colloidal rods that catalyze hydrogen peroxide redox, are attracted by a hydrogen peroxide source. Under such conditions, JPs act as molecular “robots” and can thus be employed in practical applications, such as the design of new intelligent drugs [6]. More sophisticated chemical robots have been proposed that utilize artificial chemotaxis to navigate autonomously [7].

The simplest and, possibly, best established model of self-propulsion is encoded by the Langevin equations [9–12]

$$\begin{aligned} \dot{x} &= v_0 \cos \phi + \sqrt{D_0} \xi_x(t), & \dot{y} &= v_0 \sin \phi + \sqrt{D_0} \xi_y(t), \\ \dot{\phi} &= \sqrt{D_\phi} \xi_\phi(t), \end{aligned} \quad (1)$$

where $\mathbf{r} = (x, y)$ are the coordinates of the swimmer in the plane, v_0 its self-propulsion speed, and D_ϕ an orientational diffusion constant, whose reciprocal, τ_ϕ , quantifies the time-persistency of the particle’s Brownian motion. Here, $\xi_i(t)$, with $i = x, y, \phi$, are zero-mean and δ -correlated Gaussian noises with $\langle \xi_i(t) \xi_j(0) \rangle = 2\delta_{ij} \delta(t)$. For long observation times t , with $t \gg \tau_\phi$, or lengths l , with $l \gg l_\phi \equiv v_0 \tau_\phi$, the effective diffusion constant, D , defined by the asymptotic law $\lim_{t \rightarrow \infty} \langle \mathbf{r}^2(t) \rangle = 4Dt$ [13], is $D = D_0 + D_s$, where D_0 is due to thermal fluctuations in the suspension, and $D_s = v_0^2/2D_\phi$ is a (typically) much larger self-propulsion term, which depends on the chemical composition of the suspension itself.

Let us consider now a chemical reactor consisting of a narrow, straight channel of length L oriented along the x

axis, and a free JP moving in it (Fig. 1) [8]. A constant concentration gradient of the chemical that fuels the particle’s self-propulsion is maintained by connecting the channel to two reservoirs in thermal equilibrium with concentrations $\rho_L < \rho_R$. The chemical concentration in the channel, $\rho(x)$, will then grow linearly from left to right. At the channel ends, $x = \pm L/2$, two porous membranes allow the chemical flow in and out but prevent the JP from escaping into the reservoirs. We speculate, based on experimental observations [9,14–16], that both v_0 and D_ϕ (and therefore D_s) may depend on $\rho(x)$ to some unspecified extent. We only assume that both $v_0(x)$ and $D_\phi(x)$ are nondecreasing functions of the channel coordinate x . Indeed, a higher fuel concentration typically enhances active Brownian motion. For this reason, the right and left channel endpoints are termed, respectively, hot and cold. We then ask ourselves two closely related questions. Upon injecting the JP at the center of the channel, $x = 0$: (1) Which containment membrane is the JP more likely to hit first? (2) On which side of the channel is it going to sojourn the most time?

This might sound paradoxical, but we came to the conclusion that the injected JP is finally attracted toward the left (cold) exit, even if, immediately after injection, it may drift to either direction, depending on the x -dependence of the propulsion parameters v_0 and τ_ϕ . For the most common case when the x -dependence of τ_ϕ is much weaker than D_s [9,14–16], the injected particle points decidedly to the right (hot) exit. Reconciling these seemingly conflicting mechanisms is of paramount importance to control the chemotaxis of artificial microswimmers as opposed to bacterial chemotaxis [17,18]. To avoid misunderstandings we remark that the adjectives hot and cold refer here to the regions in the reactor where the effective swimmer diffusion due to the selfpropulsion, $D_s(x)$, is the highest and lowest, respectively. The thermal diffusion, D_0 , is assumed to be x -independent, which means that thermal gradients do not enter our analysis. Accordingly, in the absence of thermal gradients and for low fuel concentrations, additional transport contributions due to hydrodynamic effects in the suspension fluid can be safely neglected.

This paper is organized as follows. In Sec. II we present numerical results for the “splitting probabilities” that a JP, injected at the center of the channel, exits it through the

*Corresponding author: yunyunli@tongji.edu.cn

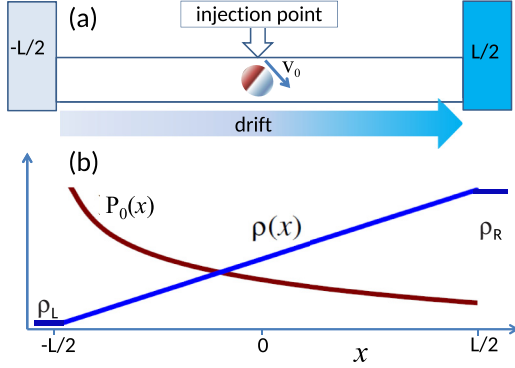


FIG. 1. (Color online) Chemical reactor with a stationary fuel concentration gradient, $\rho(x)$ (see text). A Janus particle injected in the middle (a) tends to drift to the right even if its probability density, $P_0(x)$, peaks on the left (b). The data in panel (b) are for $v_0(x) \propto \rho(x)$ with $D_0 = 0.01$, $\eta_v = 1$, $\delta_v = 1$, $\delta_\phi = 0$, and $D_\phi = 0.1$.

right or left end and the corresponding mean first-exit times. The particle clearly undergoes a transient drift toward the hot end of the channel, whereas its stationary distribution tends to accumulate at the opposite end. In Sec. III we interpret our data by means of a phenomenological 1D Langevin equation that describes the diffusion of a Brownian particle with the spatial-dependent diffusion coefficient $D_s(x)$. The spatial dependence of $D_s(x)$ generates the drift term here detected as a transient drift. Finally, in Sec. IV we discuss the implications of our findings in the interpretation of recent experiments on the diffusion of JPs in concentration gradients.

II. NUMERICAL RESULTS

Our answers to questions (1) and (2) are based on the simulation data reported in Fig. 2. As a study case, we considered the x -dependent self-propulsion parameters,

$$v_0(x) = v_0(1 + \delta_v x/L)^{\eta_v}, \quad D_\phi(x) = D_\phi(1 + \delta_\phi x/L)^{\eta_\phi}, \quad (2)$$

where $\delta_v = \Delta v_0/v_0$ and $\delta_\phi = \Delta D_\phi/D_\phi$ are both nonnegative, and from now on, v_0 and D_ϕ are shorthands for $v_0(0)$ and $D_\phi(0)$ at the injection point. We also set $\eta_v = 1$ and $\eta_\phi = 2$, so that for $\delta_v = \delta_\phi$ the self-propulsion diffusion term, $D_s(x) = v_0^2(x)/2D_\phi(x)$, is x -independent, i.e., $D_s(x) = D_s$. That is, the JP is expected to diffuse uniformly along the channel. On the contrary, we observed that the stationary probability density function (p.d.f.), $P_0(x)$, of a single JP in such a closed-ended channel tends to accumulate against the left exit, as displayed in Fig. 2(a). This effect is the strongest as δ_v is increased at $\delta_\phi = 0$. Vice versa, as δ_ϕ is raised and δ_v lowered, $P_0(x)$ tends to flatten out. For $\delta_v = 0$, no matter what δ_ϕ , $P_0(x) = L^{-1}$. Actually, the x -dependence of $D_\phi(x)$ seems not to sensibly affect $P_0(x)$ for any choice of η_ϕ [Fig. 2(a), inset]. In conclusion, to answer question (2), the injected JP tends to dwell where $v_0(x)$ is the lowest, as suggested in Ref. [17], that is by the cold extremity of the channel (reverse chemotaxis).

When one looks at the transient dynamics immediately following the particle injection, a surprising outcome appears. We injected the particle at $x = 0$ and clocked the time it

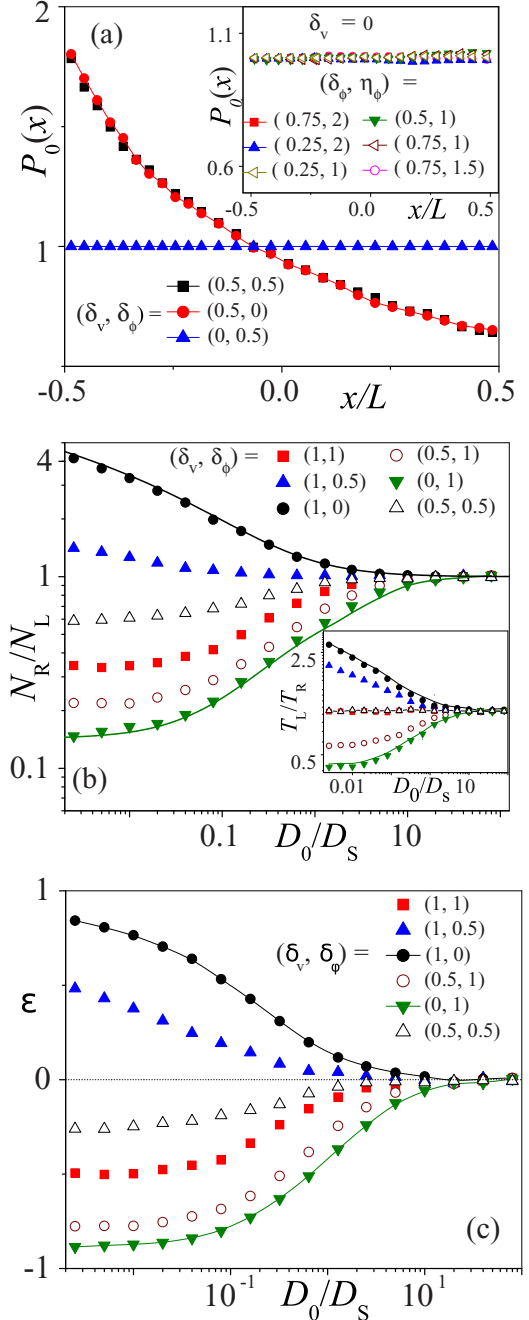


FIG. 2. (Color online) Janus particle in a concentration gradient, Eq. (2), with $\eta_v = 1$, $\eta_\phi = 2$, and different δ_ϕ and δ_v : (a) $P_0(x)$ for $D_0 = 0.01$. Data for $D_0 = 0.01$ and different η_ϕ are plotted in the inset; (b) N_R/N_L and T_L/T_R (inset) vs. D_0 ; and (c) ϵ vs. D_0 , Eq. (9). Other simulation parameters: $v_0 = 1$, $D_\phi = 1$, $L = 100l_\phi$ and channel width $y_l = 5$. The solid curves are the analytical predictions based on Eqs. (5) and (6) with $\alpha = 1/2$ and $\alpha = 1$, respectively, for $\delta_\phi = 0$ and $\delta_v = 0$.

takes to hit either the right or left containment membrane. We repeated this numerical experiment $N = 10^6$ times and determined the probability the particle first reached the right or left exit, $N_{R,L}/N$, and the corresponding mean-first-passage times (MFPT), $T_{R,L}$, from 0 to $\pm L/2$. The ratios N_R/N_L and T_L/T_R are plotted, respectively, in the main panel and the inset

of Fig. 2(b). In the regime of low thermal noise, $D_0 \ll D_s$, we obtained distinct results, depending on which x -dependence is stronger, $v_0(x)$ or $D_\phi(x)$. [Note that we used the same η_v and η_ϕ as in Fig. 2(a) for $P_0(x)$]. In the first case, the particle tries to leave the channel through the right exit and, accordingly, $T_L > T_R$. Vice versa, on suppressing the x -dependence of $v_0(x)$, while leaving $D_\phi(x)$ unchanged, the particle directs itself preferably toward to left exit and $T_L < T_R$.

This means that for $\delta_v \gg \delta_\phi$ the injected particle initially drifts up the $\rho(x)$ gradient (pseudochemotaxis), at odds with Ref. [17]. Only when the increase of $v_0(x)$ along the channel is accompanied by a suitably stronger increase of its orientational rate, D_ϕ , the injected particle drifts immediately down the gradient, in agreement with Fick's law for ordinary Brownian motion. Magnitude and orientation of the transient drift are characterized in the forthcoming section by means of the unique rectification factor ϵ . This result is remarkable because $P_0(x)$ tends to accumulate in any case around the concentration minima. This behavior is reminiscent of the ‘‘drift without current’’ effect experimentally observed in Ref. [19,20] and numerically investigated in Ref. [21] for thermal Brownian motion in confined geometries. However, the magnitude of the phenomenon reported here is significantly larger and more easily accessible to experimental demonstration.

III. PHENOMENOLOGICAL ANALYSIS

An analytical treatment of the model of Eq. (1) is viable in two limiting cases, i.e., $\delta_\phi = 0$, $\delta_v > 0$, and $\delta_v = 0$, $\delta_\phi > 0$. For this purpose we implemented the approach of Ref. [22] to reduce the fully three-dimensional dynamics of Eq. (1) to the more tractable 1D phenomenological diffusion law,

$$\dot{x} = \alpha D'_\alpha(x) + \sqrt{D_\alpha(x)}\xi(t), \quad (3)$$

where the prime sign denotes an x derivation and (i) $\alpha = 1/2$ and $D_{1/2}(x) = D_0 + v_0^2(x)/2D_\phi$, for $\delta_\phi = 0$, and (ii) $\alpha = 1$ and $D_1(x) = D_0 + v_0^2/2D_\phi(x)$, for $\delta_v = 0$. Here, the multiplicative noise term has to be handled according to Ito's prescription [13] and $\xi(t)$ is defined like the noises of Eq. (1). Note that the Eq. (3) can be rewritten as $\dot{x} = \sqrt{D_\alpha(x)} \circ \xi(t)$, with \circ denoting the Stratonovitch or anti-Ito prescription, respectively, in cases (i) and (ii). The corresponding Fokker-Planck equation (FPE) is

$$\begin{aligned} \frac{\partial}{\partial t} P(x,t) &= \frac{\partial}{\partial x} \left[-v_\alpha(x) + \frac{\partial}{\partial x} D_\alpha(x) \right] P(x,t) \\ &= -\frac{\partial}{\partial x} j(x,t), \end{aligned} \quad (4)$$

with $v_\alpha(x) = \alpha D'(x)$ for the appropriate value of α [17,23]. The stationary p.d.f. for zero net current, $j_0 \equiv \lim_{t \rightarrow \infty} j(x,t) = 0$, reads

$$P_0(x) = \lim_{t \rightarrow \infty} P(x,t) = \mathcal{N}/D_\alpha(x)^{1-\alpha}, \quad (5)$$

where \mathcal{N} is a normalization constant. In particular, for $\alpha = 1$, i.e., x -independent v_0 , $P_0(x) = 1/L$. The extension to cases with $j_0 \neq 0$ is straightforward.

Regarding the transient statistics of a particle injected at the center of the channel, $x = 0$, a simple ‘‘splitting probability’’

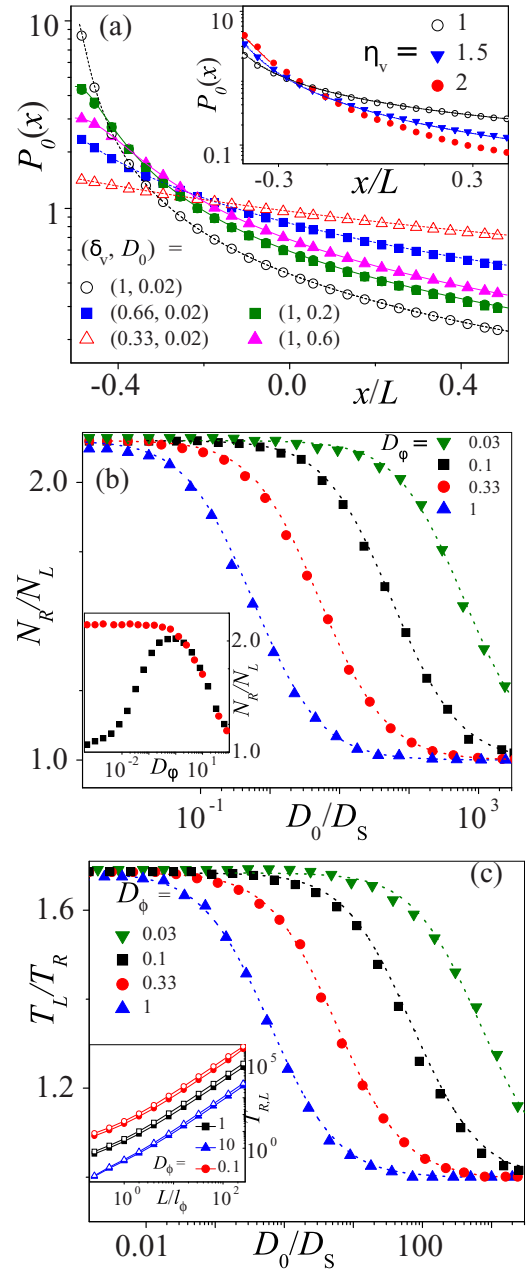


FIG. 3. (Color online) Channel diffusion for $\eta_v = 1$ and $\delta_\phi = 0$: (a) $P_0(x)$ for $D_\phi = 0.1$, $v_0 = 1.5$, and different δ_v and D_0 (see legends). Inset: $P_0(x)$ for $D_0 = 0.02$, $D_\phi = 0.1$, $\delta_v = 1$, and different η_v ; (b) N_R/N_L vs. D_0 for $\delta_v = 2/3$ and different D_ϕ ; and (c) T_L/T_R vs. D_0 for $\delta_v = 2/3$ and different D_ϕ . Other simulation parameters are: $v_0 = 1.5$, $L = 100l_\phi$, and channel width $y_l = 5$. Inset in panel (b): N_R/N_L vs. D_ϕ for $D_0 = 0.03$ and $L = 100$ (squares) and $100l_\phi$ (circles). Inset in panel (c): T_L/T_R vs. L/l_ϕ for $D_0 = 0.03$, and different D_ϕ . The remaining simulation parameters are as in the relevant main panel. Dashed and solid curves are the corresponding analytical predictions based on Eqs. (5) and (6) for $\alpha = 1/2$.

calculation [13] leads to

$$\frac{N_R}{N} = \frac{\int_{-L/2}^0 [D_\alpha(x)P_0(x)]^{-1} dx}{\int_{-L/2}^{L/2} [D_\alpha(x)P_0(x)]^{-1} dx}. \quad (6)$$

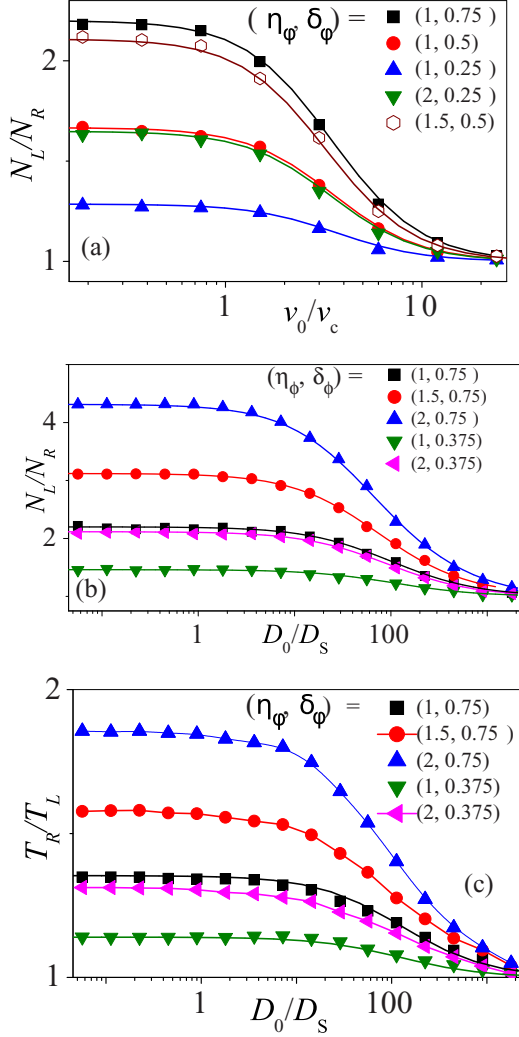


FIG. 4. (Color online) Channel diffusion for $\delta_v = 0$ and different δ_ϕ and η_ϕ (in legends): (a) N_R/N_L vs. v_0 for $D_0 = 0.03$; (b) N_R/N_L vs. D_0 for $v_0 = 1.5$; and (c) T_L/T_R vs. D_0 for $v_0 = 1.5$. In (a)–(c) $D_\phi = 0.1$, $L = 100l_\phi$, and $\gamma_L = 5$. The solid curves are the corresponding analytical predictions based on Eqs. (5) and (6) for $\alpha = 1$.

with $N_R + N_L = N$. Analogously, for the MFPTs in a channel with absorbing endpoints, we have [13]

$$T_L(\delta_\alpha) = \langle \tilde{T}(x) \rangle_{(0,L/2)} - \langle \tilde{T}(x) \rangle_{(-L/2,L/2)} = T_R(-\delta_\alpha), \quad (7)$$

where $\delta_{1/2} = \delta_v$ and $\delta_1 = \delta_\phi$,

$$\tilde{T}(x) = \int_{-L/2}^x dz \psi_\alpha(z) / D_\alpha(z) \int_z^{L/2} dy / \psi_\alpha(y),$$

and $\langle \dots \rangle_{(a,b)} = \int_a^b \langle \dots \rangle dx / \psi_\alpha(x) / \int_a^b dx / \psi_\alpha(x)$, with $\psi_\alpha(x) = [D_\alpha(x)]^\alpha$. The second equality in Eq. (7) follows immediately from $x \rightarrow -x$ symmetry considerations. The ratios N_R/N_L and T_L/T_R have been computed numerically. The results plotted for $\alpha = 1/2$ (Fig. 3) and for $\alpha = 1$ (Fig. 4) confirm the consistency of our phenomenological approach in both regimes.

Clearly, our approach hinges on the phenomenological Eq. (3) and the explicit expressions we used for v_α and $D_\alpha(x)$. We now justify our choice for both.

(i) $\delta_\phi = 0$, $\delta_v > 0$. In view of the third equation (1), we know that $\cos \phi(t)$ behaves like a (non-Gaussian) colored noise with an asymptotic autocorrelation function $\langle \cos \phi(t) \cos \phi(0) \rangle \simeq (1/2)e^{-D_\phi|t|}$ for $t \gg \tau_\phi$ [24]. The JP diffusion coefficient at x can thus be derived from Kubo's formula [12,23],

$$D = D_0 + \lim_{t \rightarrow \infty} \int_0^t v_0^2(x) \langle \cos \phi(t) \cos \phi(0) \rangle dt = D_{1/2}(x),$$

as anticipated in Eq. (3).

The drift velocity, $v_\alpha(x)$, of a JP with an x -independent self-propulsion time constant, τ_ϕ , amounts to the average of $v_0(x)$ over its persistence length $l_\phi(x) = v_0(x)\tau_\phi$, i.e.,

$$v_\alpha(x) = \frac{1}{2} \left[v_0 \left(x + \frac{l_\phi}{2} \right) - v_0 \left(x - \frac{l_\phi}{2} \right) \right] \simeq \frac{1}{2} v_0'(x) v_0(x) \tau_\phi, \quad (8)$$

hence $v_\alpha = \alpha D_\alpha'(x)$ as in Eq. (4) with $\alpha = 1/2$.

(ii) $\delta_\phi > 0$, $\delta_v = 0$. Calculating $D(x)$ in this case is straightforward. The FPE corresponding to the first and third Langevin Eq. (1),

$$\frac{\partial}{\partial t} \bar{P} = \left[-v_0 \cos \phi \frac{\partial}{\partial x} + D_0 \frac{\partial^2}{\partial x^2} + D_\phi(x) \frac{\partial^2}{\partial \phi^2} \right] \bar{P},$$

with $\bar{P} = \bar{P}(x, \phi, t)$, admits a uniform p.d.f., as one can prove by substitution; hence, the $P_0(x)$ of Eq. (5) with $\alpha = 1$. The diffusion coefficient will be calculated again through Kubo's formula: since in the stationary regime x and t are statistically independent, $D = D_1(x)$. Regarding the drift velocity, the condition $j_0 = 0$ in Eq. (3) requires that $v_\alpha(x) = D_\alpha(x) (\ln[D_\alpha(x)P_0(x)])'$, namely, for $\alpha = 1$, $v_1(x) = D_1'(x)$, as expected.

Coming back to the plots of Figs. 3 and 4, we stress that:

(i) The insets of Figs. 3(b) and 3(c) illustrate the dependence of $N_{R,L}$ and $T_{R,L}$ on the channel length L : $T_{R,L}$ scale like L^2 , whereas $N_{R,L}$ grow insensitive to L . Of course, both statements are valid as long as $L \gg l_\phi$;

(ii) Our expressions for $T_{L,R}(\delta_\alpha)$, adapted from Ref. [13], correctly reproduce the limiting values $T_{R,L}(\delta_\alpha) = L^2/8D_0$ for $D_0 \ll D_s$ (gradient effects are superseded by thermal noise), and $T_{R,L}(0) = L^2/8D_s$ for $D_0 = 0$ and $\delta_\alpha \rightarrow 0$ (purely active Brownian motion);

(iii) On comparing the curves for N_R/N_L in Figs. 3(b) and 4(b) and those for T_L/T_R in Figs. 3(c) and 4(c), the different dependence of the two ratios on D_ϕ at low thermal noise becomes apparent. This can be easily explained by inspecting the corresponding analytical expressions in the limit $D_0 \rightarrow 0$. For $\delta_\phi = 0$, $\delta_v > 0$, i.e., $\alpha = 1/2$, the two ratios are functions of δ_v only and, therefore, independent of D_ϕ . For $\delta_v = 0$, $\delta_\phi \neq 0$, i.e., $\alpha = 1$, they grow insensitive to v_0 , but do depend on δ_ϕ and, hence, D_ϕ . Accordingly, the limits $D_0 \rightarrow 0$ and $v_0 \rightarrow \infty$ coincide, as confirmed, for instance, by the numerical data in Figs. 4(a) and 4(b).

Finally, to fully answer our starting question (1), as the most likely exit end in the general case $\delta_v \neq 0$ and $\delta_\phi \neq 0$, we computed the rectification factor,

$$\epsilon \equiv \langle v_\alpha(0) \rangle / v_0 = \left(\frac{N_R}{N_L} \frac{T_L}{T_R} - 1 \right) / \left(\frac{N_R}{N_L} \frac{T_L}{T_R} + 1 \right), \quad (9)$$

where the ratios N_R/N_L and T_L/T_R are combined together to quantify both the sign and magnitude of the symmetry-breaking mechanism responsible for the pseudochemotactic drifts. The most effective right (left) rectification corresponds to $\epsilon = \pm 1$, whereas for $\epsilon = 0$ the opposite pulls by $v_0(x)$ and $D_\phi(x)$ cancel each other. Note that for $\eta_v = 1$, $\eta_\phi = 2$, and $\delta_v = \delta_\phi$, the transient rectification does not vanish [Fig. 2(c)], even if under the same conditions $T_L = T_R$ [Fig. 2(b), inset].

IV. CONCLUDING REMARKS

The phenomenon of “drift without current” has been explained in Refs. [19,25] using the phenomenological Eq. (3), by noticing that the statistical ensemble governing the average drift (i.e., the rectification factor ϵ in our notation) is different from the one required to compute the average current, $j_0 = 0$. The former consists of the representative points exiting an infinitesimally narrow neighborhood with coordinate x , with equal x -dependent jump length in either direction, whereas the latter consists of all points crossing a channel cross-section with coordinate x at a given time, no matter what their jumping length. The two ensembles differ as an effect of multiplicative noise [i.e., the x -dependence of $D_\alpha(x)$] and so do the currents thus calculated.

Self-propelling artificial microswimmers reproduce that very same situation as a combined effect of nonequilibrium and the higher dimensionality of their dynamics, Eq. (1). In contrast to bacterial chemotaxis [17], for an artificial microswimmer the self-propulsion parameters do not depend on the orientation. Here a dependence on the swimmer’s orientation might come into play due to, say, inertial or memory (i.e., nonlocal) effects, but surely not to some internal sensor-actuator pathways, like in bacteria [1]. The microswimmers considered here are characterized by very

low Reynolds numbers and small dimensions compared to the $\rho(x)$ length scale; therefore, an orientation dependence of the swimmer’s self-propulsion mechanism is not an option.

For artificial microswimmers under the most common experimental conditions, D_ϕ is only weakly affected by the ρ gradient, while $v_0(x)$ is reported to grow linearly with ρ and then saturate at higher ρ [9,14–16]. The onset of “anti-Fick” cold-to-hot (pseudochemotactic) currents can thus be easily demonstrated. For instance, a source steadily releasing fuel into a JP suspension causes a concentration gradient around it; JPs with x -independent rotational dynamics are driven away from the fuel source, whereas a tagged JP floating in such a depletion zone actually drifts toward the source. This prediction is in contrast with the experimental findings of Ref. [4], where Au-Pt microrods are reported to progressively cluster around an H_2O_2 fuel source. If we assume that the self-propulsion model of Eq. (1) holds good for a free swimmer in the bulk (as established under the most diverse experimental conditions [9,11,26]), the only explanation for such a discrepancy is that, upon migrating toward the fuel source, the JPs come into contact with one another and eventually aggregate, as suggested, e.g., in Ref. [27]. Drifts without current become observable at low swimmer concentration.

ACKNOWLEDGMENTS

We thank RIKEN’s RICC for computational resources. Y.L. is supported by the National Natural Science Foundation of China under Grant No. 11334007, and by Tongji University under Grant No. 2013KJ025. P.K.G. is partly supported by the UGC-BSR start-up Grant No. F.30-92/2015. F.N. is partly supported by the RIKEN iTHES Project, the MURI Center for Dynamic Magneto-Optics, and a Grant-in-Aid for Scientific Research (S).

-
- [1] H. C. Berg, *E. coli in Motion* (Springer, New York, 2004).
- [2] F. Schweitzer, *Brownian Agents and Active Particles* (Springer, Berlin, 2003).
- [3] S. Jiang, Q. Chen, M. Tripathy, E. Luijten, K. S. Schweizer, and S. Granick, *Adv. Mater.* **22**, 1060 (2010); A. Walther and A. H. E. Müller, *Chem. Rev.* **113**, 5194 (2013).
- [4] Y. Hong, N. M. K. Blackman, N. D. Kopp, A. Sen, and D. Velegol, *Phys. Rev. Lett.* **99**, 178103 (2007).
- [5] S. Sengupta, K. K. Dey, H. S. Muddana, T. Tabuillot, M. E. Ibele, P. J. Butler, and A. Sen, *JACS* **135**, 1406 (2013).
- [6] S. Sengupta, M. E. Ibele, and A. Sen, *Angew. Chem. Int. Ed. Engl.* **51**, 8434 (2012).
- [7] I. Lagzi, *Cent. Eur. J. Med.* **8**, 377 (2013).
- [8] See, e.g., P. S. Burada, P. Hänggi, F. Marchesoni, G. Schmid, and P. Talkner, *ChemPhysChem* **10**, 45 (2009).
- [9] J. G. Gibbs and Y.-P. Zhao, *Appl. Phys. Lett.* **94**, 163104 (2009); J. R. Howse, R. A. L. Jones, A. J. Ryan, T. Gough, R. Vafabakhsh, and R. Golestanian, *Phys. Rev. Lett.* **99**, 048102 (2007).
- [10] S. van Teeffelen and H. Löwen, *Phys. Rev. E* **78**, 020101 (2008).
- [11] G. Volpe, I. Buttinoni, D. Vogt, H.-J. Kümmerer, and C. Bechinger, *Soft Matter* **7**, 8810 (2013).
- [12] For a minireview see X. Ao, P. K. Ghosh, Y. Li, G. Schmid, P. Hänggi, and F. Marchesoni, *Eur. Phys. J. Special Topics* **223**, 3227 (2014).
- [13] C. W. Gardiner, *Handbook of Stochastic Methods* (Springer, Berlin, 1985).
- [14] A. Sen, M. Ibele, Y. Hong, and D. Velegol, *Faraday Discuss.* **143**, 15 (2009).
- [15] Y. Hong, D. Velegol, N. Chaturvedi, and A. Sen, *Phys. Chem. Chem. Phys.* **12**, 1823 (2010).
- [16] F. Lugli, E. Brini, and F. Zerbetto, *J. Phys. Chem. C* **116**, 592 (2012).
- [17] M. J. Schnitzer, *Phys. Rev. E* **48**, 2553 (1993).
- [18] D. A. Clark and L. C. Grant, *Proc. Natl. Acad. Sci. USA* **102**, 9150 (2004).
- [19] P. Lançon, G. Batrouni, L. Lobry, and N. Ostrowsky, *Europhys. Lett.* **54**, 28 (2001); *Physica A* **304**, 65 (2001).
- [20] G. Volpe, L. Helden, T. Brettschneider, J. Wehr, and C. Bechinger, *Phys. Rev. Lett.* **104**, 170602 (2010).
- [21] P. F. Tupper and X. Yang, *Proc. R. Soc. A* **468**, 3864 (2012); R. Collins and T. Takemori, *J. Phys. Condens. Matter* **1**, 3801 (1989).
- [22] F. Marchesoni, *Materials* **6**, 3598 (2013), and references therein.

- [23] C. Festa, L. Fronzoni, P. Grigolini, and F. Marchesoni, *Phys. Lett. A* **102**, 95 (1984).
- [24] P. K. Ghosh, V. R. Misko, F. Marchesoni, and F. Nori, *Phys. Rev. Lett.* **110**, 268301 (2013).
- [25] M. Yang and M. Ripoll, *J. Chem. Phys.* **136**, 204508 (2012).
- [26] D. Takagi, A. B. Braunschweig, J. Zhang, and M. J. Shelley, *Phys. Rev. Lett.* **110**, 038301 (2013).
- [27] Y. Fily and M. C. Marchetti, *Phys. Rev. Lett.* **108**, 235702 (2012).